

Low-temperature spray-deposited indium oxide for flexible thin-film transistors and integrated circuits

Luisa Petti, Hendrik Faber, Niko Münzenrieder, Giuseppe Cantarella, Panos A. Patsalas, Gerhard Tröster, and Thomas D. Anthopoulos

Citation: *Applied Physics Letters* **106**, 092105 (2015); doi: 10.1063/1.4914085

View online: <http://dx.doi.org/10.1063/1.4914085>

View Table of Contents: <http://scitation.aip.org/content/aip/journal/apl/106/9?ver=pdfcov>

Published by the [AIP Publishing](#)

Articles you may be interested in

[Low-voltage polymer/small-molecule blend organic thin-film transistors and circuits fabricated via spray deposition](#)

Appl. Phys. Lett. **106**, 223304 (2015); 10.1063/1.4922194

[High stability mechanisms of quinary indium gallium zinc aluminum oxide multicomponent oxide films and thin film transistors](#)

J. Appl. Phys. **117**, 045309 (2015); 10.1063/1.4906619

[High electron mobility thin-film transistors based on Ga₂O₃ grown by atmospheric ultrasonic spray pyrolysis at low temperatures](#)

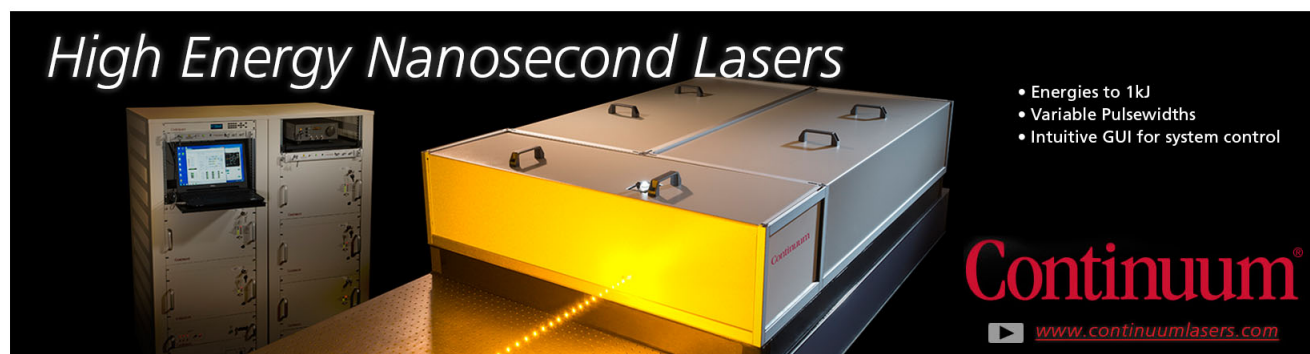
Appl. Phys. Lett. **105**, 092105 (2014); 10.1063/1.4894643

[Chemical composition and temperature dependent performance of ZnO-thin film transistors deposited by pulsed and continuous spray pyrolysis](#)

J. Appl. Phys. **114**, 234502 (2013); 10.1063/1.4846736

[Cadmium sulfide thin-film transistors fabricated by low-temperature chemical-bath deposition](#)

J. Appl. Phys. **96**, 5819 (2004); 10.1063/1.1804244

An advertisement for Continuum High Energy Nanosecond Lasers. The image shows a large, industrial-grade laser system with a prominent yellow glow from the laser output. To the left, there is a control console with a monitor and various buttons. The background is dark, making the laser and control console stand out. The text 'High Energy Nanosecond Lasers' is written in a white, serif font at the top left. On the right side, there is a list of features: 'Energies to 1kJ', 'Variable Pulsewidths', and 'Intuitive GUI for system control'. The Continuum logo is at the bottom right, with the website address 'www.continuumlasers.com' below it.

High Energy Nanosecond Lasers

- Energies to 1kJ
- Variable Pulsewidths
- Intuitive GUI for system control

Continuum[®]

www.continuumlasers.com

Low-temperature spray-deposited indium oxide for flexible thin-film transistors and integrated circuits

Luisa Petti,¹ Hendrik Faber,¹ Niko Münzenrieder,² Giuseppe Cantarella,² Panos A. Patsalas,³ Gerhard Tröster,² and Thomas D. Anthopoulos^{1,a)}

¹Blackett Laboratory, Department of Physics and Centre for Plastic Electronics, Imperial College London, London SW7 2BW, United Kingdom

²Electronics Laboratory, Swiss Federal Institute of Technology Zurich, Gloriastrasse 35, 8092 Zurich, Switzerland

³Department of Physics, Laboratory of Applied Physics, Aristotle University of Thessaloniki, GR-54124 Thessaloniki, Greece

(Received 14 December 2014; accepted 22 February 2015; published online 6 March 2015)

Indium oxide (In₂O₃) films were deposited by ultrasonic spray pyrolysis in ambient air and incorporated into bottom-gate coplanar and staggered thin-film transistors. As-fabricated devices exhibited electron-transporting characteristics with mobility values of 1 cm²V⁻¹s⁻¹ and 16 cm²V⁻¹s⁻¹ for coplanar and staggered architectures, respectively. Integration of In₂O₃ transistors enabled realization of unipolar inverters with high gain (5.3 V/V) and low-voltage operation. The low temperature deposition (<250 °C) of In₂O₃ also allowed transistor fabrication on free-standing 50 μm-thick polyimide foils. The resulting flexible In₂O₃ transistors exhibit good characteristics and remain fully functional even when bent to tensile radii of 4 mm. © 2015 AIP Publishing LLC.

[<http://dx.doi.org/10.1063/1.4914085>]

Thin-film transistors (TFTs) based on transparent metal oxide semiconductors^{1,2} hold great promise for a host of future large-area, large-volume electronic applications including flexible radio frequency identification (RFID) tags,³ flexible and paper-like displays,⁴ and electronic skin.⁵ To this end, recent years have witnessed the development of a range of high-mobility metal oxide semiconductors and devices that can be manufactured over large areas employing simple and low-temperature fabrication methods.⁶ Among the various deposition techniques demonstrated, solution processing offers a scalable and cost effective route for high throughput and large-area deposition of various oxide materials including ZnO, In₂O₃, SnO₂, and SnO, to name a few.^{7,8} Among those, In₂O₃—a simple binary metal oxide—has attracted an increasing interest in the last years owing to its large electron mobility (up to 160 cm²V⁻¹s⁻¹ in single crystal device grown from vapor-phase at 1000 °C⁹) and the high optical transparency (>90%) given by its wide band gap (~3.1 eV⁹). A significant advantage associated with the application of In₂O₃ in thin-film devices is that it can be grown at relatively low temperatures employing a diverse range of vapor-phase techniques,^{10–12} as well as solution-based methods.^{13–16} To date, solution-processed In₂O₃-based devices have been demonstrated by inkjet-printing¹³ and spin-casting.^{15–18} Tremendous advances have been made to realize solution-processed TFTs at low temperatures (170–400 °C) with field-effect electron mobility values ranging from 0.01 cm²V⁻¹s⁻¹ up to 44 cm²V⁻¹s⁻¹.^{13,15–18} Despite the huge promise, however, accurate control over the morphology and the chemical composition of solution-grown In₂O₃ still remains very challenging, leading to significant device-to-device variations. Recently, spray pyrolysis (SP)

has demonstrated to be a particularly appealing technology, enabling a simple and scalable deposition of a large variety of oxide semiconductors, from n-type ZnO,^{19,20} IZO,²¹ ZTO,²² and Ga₂O₃²³ to p-type Cu₂O.²⁴ Furthermore, addition of suitable dopants in the precursor solution has also allowed the demonstration of Be-doped ZnO transistors and integrated circuits with optimized operating characteristics.²⁵ Despite the tremendous potential, however, deposition of semiconducting metal oxides by spray pyrolysis has so far been limited to high processing temperatures typically in excess of >350 °C, hence rendering the technology incompatible with inexpensive, temperature-sensitive substrate materials such as plastic. In order to overcome this rather serious bottleneck, development of new material formulations and optimized processing protocols would be needed.

Here, we report the development of low-voltage In₂O₃-based TFTs and inverters using ambient ultrasonic spray pyrolysis (SP) and indium nitrate hydrate as the precursor. Optimal process conditions enable the growth of high-quality electron-transporting In₂O₃ layers and the realization of low-voltage bottom-gate, bottom-contact (BG-BC) as well as bottom-gate, top-contact (BG-TC) TFTs with electron mobility of ~1 cm²/Vs and ~16 cm²/Vs, depending on the particular device configuration employed. Use of the application relevant BG-BC transistor architecture allows the fabrication of fully functional unipolar voltage inverters with excellent operating characteristics. Finally, by taking advantage of the moderate process temperature (~250 °C), fabrication of fully functional and bendable In₂O₃-based TFTs on plastic substrate is also demonstrated. Although the use of In-based oxide semiconductors may ultimately prove expensive for application in future large-volume electronics due to the scarcity of In, our work highlights the potential of spray pyrolysis as a viable large-area deposition tool even for flexible plastic microelectronics.

^{a)}Author to whom correspondence should be addressed. Electronic mail: t.anthopoulos@imperial.ac.uk

Bottom-gate coplanar transistors were fabricated on a 4-in. silicon substrate with $1\ \mu\text{m}$ thermally grown SiO_2 acting as isolation layer. Figure 1(a) shows the schematic device cross-section. The substrate was covered by $500\ \text{nm}$ of SiN_x grown via Plasma-enhanced chemical vapour deposition (PECVD). Next, $30\ \text{nm}$ -thick e-beam evaporated Cr was structured into bottom-gate contacts using standard photolithographic etching. Following, a $25\ \text{nm}$ -thick Al_2O_3 gate dielectric layer (dielectric constant: 9.5) was deposited by atomic layer deposition (ALD) at 150°C . Gate contact holes through the Al_2O_3 were patterned by photolithography and wet chemistry.²⁶ Subsequently, $10\ \text{nm}/60\ \text{nm}$ of Ti/Au were e-beam evaporated and structured into source/drain (S/D) contacts using a lift-off process. Prior to the semiconductor deposition, the substrate was diced into chips of $1.5 \times 1.5\ \text{cm}^2$. The diced chips were then cleaned by ultra-sonication in acetone and IPA for 5 min, and submitted to 30 min UV/ozone treatment. The In_2O_3 deposition was carried out by ultrasonic spray pyrolysis using a $30\ \text{mg ml}^{-1}$ indium nitrate hydrate ($\text{In}(\text{NO}_3)_3 \cdot \text{H}_2\text{O}$) in deionized water solution. The deposition was performed in ambient air at 250°C . The resulting transistors have channel length (L) and width (W) of $10\ \mu\text{m}$ and $500\ \mu\text{m}$, respectively. Bottom-gate, staggered transistors [Figure 1(b)] were fabricated onto doped Si^{++} wafers acting as the common gate electrode with a $400\ \text{nm}$ -thick SiO_2 layer as the gate dielectric. In_2O_3 was processed using the identical process protocols followed by the thermal evaporation of top Al source/drain electrodes in high vacuum ($10^{-6}\ \text{mbar}$). X-ray diffraction (XRD) in Bragg-Brentano geometry were performed using a Bruker D8-Advance X-ray diffractometer. The surface morphology of the films was investigated by intermittent contact mode atomic force microscopy (AFM). Electrical measurements were performed in nitrogen atmosphere using a semiconductor parameter analyser. Finally, the charge carrier field-effect mobility values were extracted using the standard gradual channel approximation model.²⁷

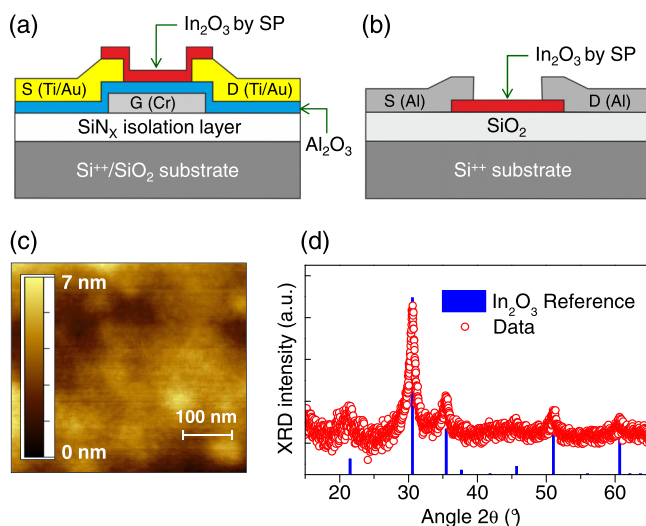


FIG. 1. Schematic cross-sections of (a) the coplanar, bottom-gate, bottom-contact and (b) staggered bottom-gate, top-contact indium oxide (In_2O_3) TFTs fabricated on Si/SiO_2 substrates. (c) AFM surface topography image of an In_2O_3 film processed on $\text{Si}/\text{SiO}_2/\text{SiN}_x/\text{Cr}/\text{Al}_2\text{O}_3$ substrate. (d) XRD diffraction patterns of spray-deposited In_2O_3 layers in comparison with peak positions of reference powder diffraction file (JCPDS-PDF 06-0416).

Figure 1(c) shows a representative AFM image of the surface topography of a $\sim 15\ \text{nm}$ -thick In_2O_3 film processed on a $\text{Si}^{++}/\text{SiO}_2$ substrate by ultrasonic SP in air. The film appears continuous and extremely smooth with a root mean square (rms) surface roughness of $\sim 1.1\ \text{nm}$. To investigate whether the as-process In_2O_3 films are amorphous, we performed XRD measurements on the same films. Figure 1(d) displays the measured XRD spectrum of a $\sim 15\ \text{nm}$ -thick spray-deposited In_2O_3 layer together with the reference powder diffraction file (JCPDS-PDF 06-0416) for comparison. It can be seen that In_2O_3 films are clearly polycrystalline as the diffraction peaks are in good agreement with the reference powder diffraction data. The mean crystallite size was also calculated from the (222) peak at around 30.5° using the Scherrer method yielding a value of $\sim 9.3\ \text{nm}$.

In order to investigate the charge transport properties of as-deposited In_2O_3 films, we fabricated coplanar BG-BC transistors [Figure 1(a)] and electrically characterise them in nitrogen at room temperature. Figures 2(a) and 2(b) display representative sets of the output and transfer characteristics measured for an In_2O_3 TFT, respectively. All devices operate at low voltages ($\leq 8\ \text{V}$) and exhibit electron transporting (n-channel) behaviour with clear channel current saturation. The devices show current on/off ratio ($I_{\text{ON}}/I_{\text{OFF}}$) of $>10^4$, threshold voltages (V_{TH}) around $\sim 2.5\ \text{V}$, sub-threshold swing (SS) of $\sim 0.9\ \text{V/dec}$, and linear (μ_{LIN}) and saturation (μ_{SAT}) field-effect mobilities of $0.6\ \text{cm}^2\text{V}^{-1}\text{s}^{-1}$ and

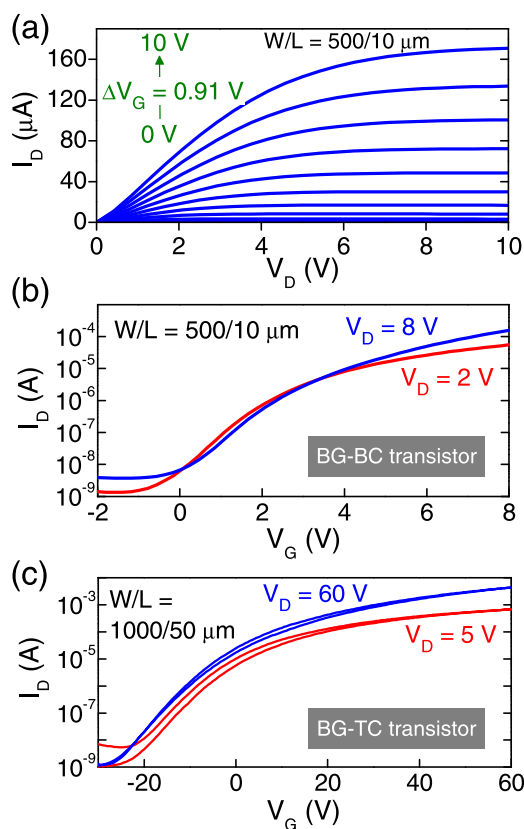


FIG. 2. (a) Output and (b) transfer characteristic of a coplanar bottom-gate, bottom-contact In_2O_3 TFT fabricated on Si/SiO_2 substrate by spray-pyrolysis in air. The channel dimensions for this device were $W/L = 500/10\ \mu\text{m}$. (c) Representative transfer characteristics measured for a staggered bottom-gate, top-contact In_2O_3 TFT fabricated on Si/SiO_2 employing Al S/D electrodes. The channel dimensions for this device were $W/L = 1000/50\ \mu\text{m}$.

$1.25 \text{ cm}^2 \text{ V}^{-1} \text{ s}^{-1}$, respectively. The mobility values obtained here are generally lower than values reported previously for solution-processed In_2O_3 transistors with comparable high- k dielectrics.^{15,16} This is primarily attributed to the unfavourable coplanar BG-BC transistor architecture and the high work function gold S/D electrodes (-5 eV) used.²⁸ When similar spray-deposited In_2O_3 channel layers were employed in staggered bottom-gate, top-contact (BG-TC) device structures [Figure 1(b)] in combination with low work function Al S/D electrodes, the electron mobility reached values up to $16 \text{ cm}^2/\text{Vs}$ [Figure 2(c)]. Although the latter value is approximately one order of magnitude lower than the Hall electron mobilities reported for single crystals of In_2O_3 prepared at 1000°C ,⁹ it is amongst the highest field-effect mobilities reported to date for In_2O_3 TFTs prepared from solution at comparable temperatures. Despite the improved performance, however, the staggered BG-TC device architecture is not practical for use in integrated circuits due to the significant complexity associated with the manufacturing and the chemically unstable nature of the low work function Al electrodes.

Because of these practical issues, we explored the use of coplanar BG-BC In_2O_3 TFTs for fabricating integrated circuits such as unipolar logic NOT gates (Figure 3). Preliminary discrete transistor characterization was used to design NOT gates with centred midpoint voltage $V_M \approx V_{DD}/2$. The inset in Figure 3 displays the schematic diagram of the inverter. The circuit comprises one driving In_2O_3 TFT with W/L of $1400/20 \mu\text{m}$

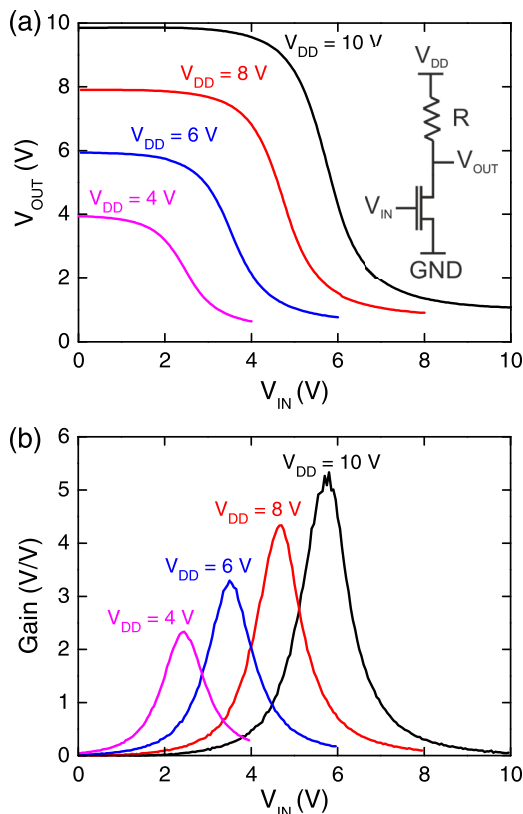


FIG. 3. (a) Voltage transfer characteristic of an In_2O_3 -based unipolar voltage inverter (NOT gate) on Si/SiO_2 substrate, measured at different supply voltages (V_{DD}). The inset shows a schematic of the inverter circuitry used. The inverter comprises a driving In_2O_3 TFT with $W = 1400 \mu\text{m}$ and $L = 20 \mu\text{m}$ and a passive load with resistance $R = 160 \text{ k}\Omega$. (b) Corresponding gains calculated from the voltage transfer characteristics.

and one passive load resistor $R = 160 \text{ k}\Omega$. The inverter was fabricated with the same process used for single TFTs, with the exception that the circuit interconnect lines were integrated directly into the source/drain metallization layer. The required resistor was implemented using the gate metal (Cr, $1.16 \times 10^{-6} \Omega\text{m}$), thereby no additional process steps were needed. Figure 3(a) and 3(b) show the voltage transfer characteristic (VTC) and the corresponding gain of the unipolar inverter measured at different supply voltages (V_{DD}) of 4, 6, 8, and 10 V. The inverter exhibits a gain >2 , even at a low $V_{DD} = 4 \text{ V}$. At $V_{DD} = 10 \text{ V}$, the inverter yields an almost centred $V_M = 5.8 \text{ V}$, and a gain as high as 5.3 V/V . Furthermore, the circuits show good output swing (output high voltage $V_{OH} = 9.8 \text{ V}$ and output low voltage $V_{OL} = 1.1 \text{ V}$) and wide noise margins (noise margin high $\text{NM}_H = 3.1 \text{ V}$ and noise margin low $\text{NM}_L = 3.68 \text{ V}$).

To demonstrate the compatibility of spray-deposited In_2O_3 TFTs with temperature-sensitive substrate materials such as plastic, we fabricated BG-BC In_2O_3 -transistors directly onto polyimide (PI) foils. We have chosen $50 \mu\text{m}$ -thick Kapton PI because of its stability against the chemicals used during device fabrication, its relatively low surface roughness ($\text{rms} \sim 4 \text{ nm}$), the low thermal ($12 \times 10^{-6} \text{ K}$) and humidity ($9 \times 10^{-6} \% \text{ RH}$) expansion coefficients, and its high glass transition temperature ($T_g \sim 360^\circ\text{C}$).^{29,30} The TFT fabrication on foil followed the same process steps employed on Si/SiO_2 substrates. The inset in Figure 4(a) shows the schematic device cross-section of the flexible In_2O_3 TFTs. To provide a sufficient adhesion of the Cr gate metal and the Al_2O_3 gate isolator to the polyimide, a 50 nm -

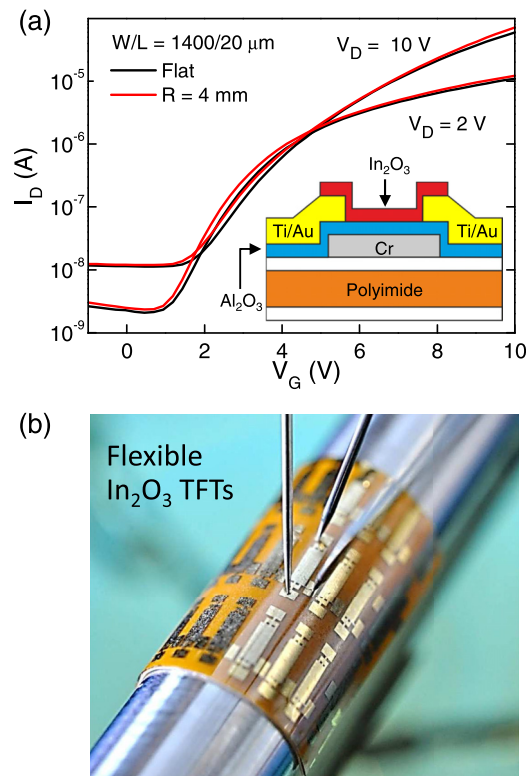


FIG. 4. (a) Transfer characteristics of spray-deposited In_2O_3 TFT fabricated on free-standing flexible polyimide foil, measured while flat and bent to a tensile radius of 4 mm . The inset shows the schematic device cross-section. The TFT dimensions are $W = 1400 \mu\text{m}$ and $L = 20 \mu\text{m}$. (b) Photograph of the actual flexible In_2O_3 TFT bent to a tensile radius of 4 mm .

thick SiN_x was deposited on both sides of the foil by PECVD. Additionally, during the spray pyrolysis process, the flexible chip was mechanically clamped on the border by employing a heavy stencil mask (mass of ~ 30 g). A typical set of transfer characteristics for a flexible In_2O_3 TFT ($W = 1400 \mu\text{m}$ and $L = 20 \mu\text{m}$) is shown in Figure 4(a). Flexible In_2O_3 TFTs exhibit good operating characteristics with an $I_{\text{ON}}/I_{\text{OFF}} = 6 \times 10^3$ ($I_{\text{OFF}} < 20$ nA), $V_{\text{TH}} = 5.29$ V, and $\mu_{\text{SAT}} = 0.2 \text{ cm}^2 \text{ V}^{-1} \text{ s}^{-1}$. The lower on/off current ratio and electron mobility of flexible TFTs, compared to devices made on Si/SiO₂ substrates, are most likely attributed to the comparatively lower thermal conductivity of the polyimide, which limits the precursor conversion during the spray process as well as the increased dielectric/semiconductor interface roughness.

Beside electrical performance, the mechanical flexibility of future TFT technologies is also expected to be a determinant factor for widespread application of the technology in flexible microelectronics. In an effort to test the effect of mechanical stress on the operating characteristics of our spray-deposited In_2O_3 TFTs, discrete devices were attached to double-sided tape and wound around a metallic rod of 4 mm radius, in a configuration that tensile strain was applied parallel to the TFT channel. Figure 4(a) shows the transfer characteristic for a typical device measured (in nitrogen) while flat and subsequently bent to a tensile radius 4 mm, which corresponds to a mechanical strain (ϵ) of $\sim 0.65\%$.³¹ Figure 4(b) displays a photograph of the actual TFT bent to 4 mm radius and contacted with the probe needles. From these measurements, it can be seen that flexible In_2O_3 TFTs are fully operational even when strained to 0.65% with only minor changes in the operating characteristics that are manifested as a negative shift in V_{TH} of -230 mV and an increased μ_{SAT} by 13%. These reversible variations are most likely related to an increase in the electron mobility and hence conductivity of In_2O_3 induced under tensile strain. This finding is in good agreement with previous reports on flexible transistors based on IGZO and IZO.^{32,33} Bending to smaller radii induces cracks in the brittle Cr gate that permanently harm the device operation.³⁴ These results demonstrate the potential of ultrasonic spray pyrolysis as a simple and scalable deposition tool for the manufacturing of flexible oxide microelectronics and certainly pave the way to future development. Combination of new precursor materials and formulations combined with improved device architectures is anticipated to lead to devices and circuits with improved performance.

In summary, we have demonstrated n-channel In_2O_3 transistors and unipolar circuits in which the semiconducting layer was deposited by ultrasonic spray pyrolysis at 250 °C. This simple and scalable method enables the fabrication of discrete transistors as well as unipolar inverters with appreciable gain (>5 V/V) and low voltage operation (≤ 10 V). The moderate deposition temperature of 250 °C used for the growth of In_2O_3 renders the method compatible with low-cost plastic substrates. This is demonstrated with the fabrication of In_2O_3 transistors on free-standing 50 μm -thick flexible polyimide foils, which exhibit good operating characteristics even when bent to 4 mm tensile radii ($\epsilon \sim 0.65\%$).

This work has been partially supported by the European Commission through the FP7 Project: Flexible multifunctional bendable integrated light-weight ultra-thin systems (FLEXIBILITY), under Contract No. FP7-287568.

- ¹J. F. Wager, D. A. Keszler, and R. E. Presley, *Transparent Electronics* (Springer, New York, 2008), p. 39.
- ²V. Subramanian and T. Lee, *Nanotechnology* **23**(34), 340201 (2012).
- ³A. Nathan, A. Ahnood, M. T. Cole, S. Lee, Y. Suzuki, P. Hiralal, F. Bonaccorso, T. Hasan, L. Garcia-Gancedo, A. Dyadyusha *et al.*, *Proc. IEEE* **100**(13), 1486 (2012).
- ⁴J. K. Jeong, *Semicond. Sci. Technol.* **26**(3), 034008 (2011).
- ⁵T. Sekitani, M. Kaltenbrunner, T. Yokota, and T. Someya, *Dig. Tech. Pap. SID Symp.* **45**(1), 122 (2014).
- ⁶Y. Sun and J. A. Rogers, *Adv. Mater.* **19**(15), 1897 (2007).
- ⁷F. Moonen, I. Yakimets, and J. Huskens, *Adv. Mater.* **24**(41), 5526 (2012).
- ⁸S. R. Thomas, P. Pattanasattayavong, and T. D. Anthopoulos, *Chem. Soc. Rev.* **42**(16), 6910 (2013).
- ⁹R. L. Weiher, *J. Appl. Phys.* **33**(9), 2834 (1962).
- ¹⁰C. Xirouchaki, G. Kiriakidis, T. F. Pedersen, and H. Fritzsche, *J. Appl. Phys.* **79**(12), 9349 (1996).
- ¹¹G. Lavareda, C. Nunes de Carvalho, E. Fortunato, A. R. Ramos, E. Alves, O. Conde, and A. Amaral, *J. Non-Cryst. Solids* **352**(23), 2311 (2006).
- ¹²R. K. Gupta, N. Mamidi, K. Ghosh, S. R. Mishra, and P. K. Kahol, *J. Optoelectron. Adv. Mater.* **9**(7), 2211 (2007).
- ¹³J. S. Lee, Y.-J. Kwack, and W.-S. Choi, *ACS Appl. Mater. Inter.* **5**(22), 11578–11583 (2013).
- ¹⁴W. Siefert, *Thin Solid Films* **120**(4), 275 (1984).
- ¹⁵M.-G. Kim, M. G. Kanatzidis, A. Facchetti, and T. J. Marks, *Nat. Mater.* **10**(5), 382 (2011).
- ¹⁶J. H. Park, Y. B. Yoo, K. H. Lee, W. S. Jang, J. Y. Oh, S. S. Chae, H. W. Lee, S. W. Han, and H. K. Baik, *Appl. Mater. Interface* **5**(16), 8067 (2013).
- ¹⁷H. S. Kim, P. D. Byrne, A. Facchetti, and T. J. Marks, *J. Am. Chem. Soc.* **130**(38), 12580 (2008).
- ¹⁸S.-Y. Han, G. S. Herman, and C.-h. Chang, *J. Am. Chem. Soc.* **133**(14), 5166 (2011).
- ¹⁹G. Adamopoulos, S. Thomas, P. H. Wöbkenberg, D. D. C. Bradley, M. A. McLachlan, and T. D. Anthopoulos, *Adv. Mater.* **23**(16), 1894 (2011).
- ²⁰H. Faber, B. Butz, C. Dieker, E. Spiecker, and M. Halik, *Adv. Funct. Mater.* **23**(22), 2828 (2013).
- ²¹S. Oertel, M. P. Jank, E. Teuber, A. Bauer, and L. Frey, *Thin Solid Films* **553**, 114 (2014).
- ²²S. Parthiban, E. Elangovan, P. K. Nayak, A. Gonçalves, D. Nunes, L. Pereira, P. Barquinha, T. Busani, E. Fortunato, and R. Martins, *J. Display Technol.* **9**(10), 825 (2013).
- ²³S. R. Thomas, G. Adamopoulos, Y. H. Lin, H. Faber, L. Sygellou, E. Stratakis, N. Pliatsikas, P. A. Patsalas, and T. D. Anthopoulos, *Appl. Phys. Lett.* **105**(9), 092105 (2014).
- ²⁴P. Pattanasattayavong, S. Thomas, G. Adamopoulos, M. A. McLachlan, and T. D. Anthopoulos, *Appl. Phys. Lett.* **102**(16), 163505 (2013).
- ²⁵S. R. Thomas, G. Adamopoulos, and T. D. Anthopoulos, *J. Display Technol.* **9**(9), 688 (2013).
- ²⁶B. Zhou and W. Ramirez, *J. Electrochem. Soc.* **143**(2), 619 (1996).
- ²⁷S. M. Sze and K. K. Ng, *Physics of Semiconductor Devices* (Wiley, New York, 2007), p. 293.
- ²⁸A. Bashir, P. H. Wöbkenberg, J. Smith, J. M. Ball, G. Adamopoulos, D. D. C. Bradley, and T. D. Anthopoulos, *Adv. Mater.* **21**(21), 2226–2231 (2009).
- ²⁹N. Münzenrieder, L. Petti, C. Zysset, T. Kinkeldei, G. A. Salvatore, and G. Tröster, *IEEE Trans. Electron Devices* **60**(9), 2815 (2013).
- ³⁰C. E. Forbes, A. Gelbman, C. Turner, H. Gleskova, and S. Wagner, *Dig. Tech. Pap. SID Symp.* **33**(1), 1200 (2002).
- ³¹H. Gleskova, S. Wagner, and Z. Suo, *JNCS* **266**, 1320 (2000).
- ³²N. Münzenrieder, K. H. Cherenack, and G. Tröster, *IEEE Trans. Electron Devices* **58**(7), 2041 (2011).
- ³³A. Dey, A. Indluru, S. M. Venugopal, D. R. Allee, and T. L. Alford, *IEEE Electron Dev. Lett.* **31**(12), 1416 (2010).
- ³⁴N. Münzenrieder, L. Petti, C. Zysset, D. Gork, L. Büthe, G. A. Salvatore, and G. Tröster, *IEEE Proc. ESSDERC* 362 (2013).